JOURNAL OF MATERIALS SCIENCE: MATERIALS IN MEDICINE **16** (2005) 1143– 1148

Crystal imperfection studies of pure and silicon substituted hydroxyapatite using Raman and XRD

SHUO ZOU, JIE HUANG, SERENA BEST, WILLIAM BONFIELD
Department of Material Science and Metallurgy, University of Cambridge, Pembroke Street, Cambridge CB2 3QZ, UK

Hydroxyapatite (HA) is important in biomedical applications because of its chemical similarity to the mineral content of bone and its consequent bioactivity. Silicon substitution into the hydroxyapatite crystal lattice was found to enhance its bioactivity both in vitro and *in vivo* [1, 2]. However, the mechanism for the enhancement is still not well understood. In this paper, the crystal imperfections introduced by silicon substitution were studied using XRD and Raman spectroscopy. It was found that silicon substitution did not introduce microstrain, but deceased the crystal size in the hk0 direction. Three new vibration modes and peak broadening were observed in Raman spectra following silicon incorporation. The imperfections introduced by silicon substitution may play a role in enhancing bioactivity. A phenomenological relationship between the width of the PO_4 $v1$ peak and crystal size was established.
© *2005 Springer Science + Business Media, Inc.*

1. Introduction

The mineral crystals in bone are calcium deficient hydroxyapatite containing a range of ion substitutes. The crystals have a plate like shape and align themselves parallel to collagen fibres along the [001] direction. Bone mineral crystals are in the order of 2–3 nm in thickness while two other dimensions are around 50 and 20 nm [3]. The nano-sized crystals contain a high density of defects. Synthetic hydroxyapatite has been used as a bone grafts since the 1970s. The similarity of hydroxyapatite to bone mineral gives rise to excellent biocompatibility, however the bioactivity of stable and well-crystallized synthetic hydroxyapatite is not as high as other bioactive materials. Silicon substitution into hydroxyapatite was found to enhance bioactivity both in vitro and *in vivo* [1, 2]. It was demonstrated that the Si-HA contains more triple junctions and more subgrain boundaries as compared to stoichiometric HA prepared and processed in a similar manner [4]. Dissolution starts from these defect sites and the enhancement in bioactivity might result from increased dissolution [5]. The defects seem to have direct implications for biological performance. It is therefore of great interest to consider material imperfections, from a crystallographic point of view. Traditionally, this quality in materials has been evaluated by imaging using SEM and TEM or by measuring crystallinity and/or crystal size using X-ray diffraction and data refinement. However, this is often a time consuming process. Also, with increasing numbers of studies on HA thin film coatings and deposited physiological apatite in SBF studies, the weakness of X-ray diffraction has been limited by peak overlap, high noise levels and low count rates due to poor crystallinity and very low thickness. Raman spectroscopy is a versatile, powerful and rapid technique and has been identified as a very useful tool in the study of both bulk and thin film apatites. In this study, FWHM (full width at half maximum) as well as the respective Guassian/Lorentzian components of the Raman peaks of SiHA/HA have been calculated using least square fitting. The correlation between the peak parameters and crystal imperfection will be discussed.

2. Materials and methods

Phase pure HA and 0.8 wt% SiHA were synthesized using a co-precipitation route described by Gibson *et al.* [1]. In the current study HA and 0.8 wt% SiHA, 1.5 and 2.0 wt% SiHA were produced and evaluated in the form of powder sintered at 1200 °C for 2 h at a ramping rate of 2.5 °C/min. X ray diffraction was used to determine the phase purity and crystallographic structure. Sintered pure HA, 0.8, 1.5 and 2.0 wt% SiHA were mixed with 10 wt% of a polycrystalline silicon standard and examined with XRD. Data were collected on a Philips PW3020 equipped with Cu $K\alpha_1/\alpha_2$ (ratio = 0.5) over a range of 10–90 deg. The step size was 0.02 deg and 10 s per step. The divergence slit/antiscatter slit were both 1/2 ° and the receiving slit was 0.2 mm. The data were then refined using Rietveld method [6] in GSAS [7] to extract the weight fraction of HA or SiHA and silicon standard. The relative crystallinity was calculated using Equation 1:

$$\text{Relative crystallinity} = (\text{wt\% HA})/(1 - 10\%) \quad (1)$$

Philips Profile fit software was used to extract the peak parameters and the Pseudo Voigt function was used to

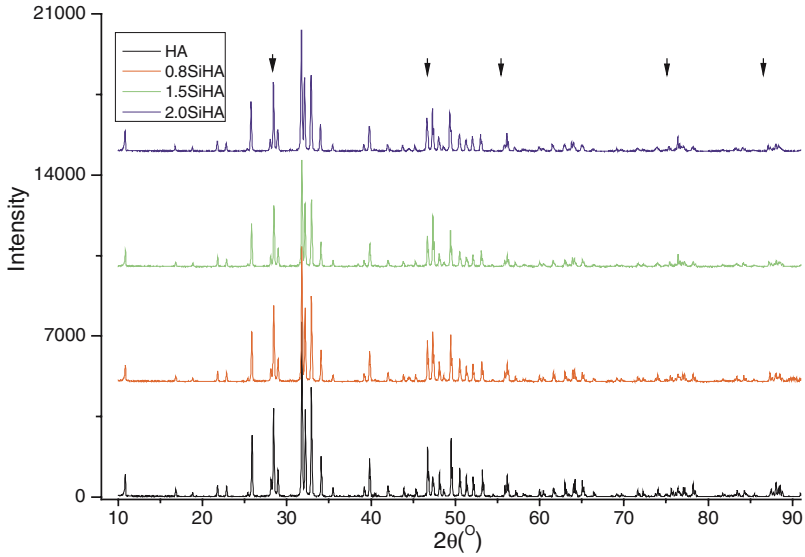

Figure 1 XRD of various HAs sintered at 1200 °C mixed with NIST Si. Major Silicon diffraction peaks are highlighted by black arrows.

model the peak shape. The $I\alpha_1/I\alpha_2$ ratio was fixed at 0.5. Amplitude, peak position, full width at half maximum (FWHM), mixing factor and asymmetry index were refined. Assuming an absence of imperfection broadening in silicon standard, the angle-dispersive instrument could be modelled using:

$$2\Gamma_{\text{inst}} = (U\tan^2\theta + V\tan\theta + W)^{1/2} \qquad (2)$$

FWHM of HA peaks ranging from 10 to 90 ° were used and the refinement of the function was performed using Origin 7 software. Williamson & Hall plots were used to separate the microstrain and crystal/domain size [8]. FWHM after correction of instrumental broadening were used for the plot. $2\sin\theta/\lambda$ (s) was plotted against $\beta_{\text{hkl}}\cos\theta/\lambda$ (Δs) where β_{hkl} is sample broadening of (hkl) plane and $\lambda = 1.5406$ Å. It is well known hydroxyapatite crystals have an anisotropic shape and the dimension along the HK0 direction was calculated with the Williamson & Hall plots. The size along the c axis was calculated by Sherrer equation using 002, 004 and 006 reflections separately assuming that no microstrain was present.

Raman spectroscopy was used to characterize the structural information for the materials. The sintered HA and Si-HA samples in powder form were placed on a glass slide and the data were collected using a Renishaw Ramascope-1000 system. The wavelength and power of the laser used were 514.5 nm and 40 mw, respectively. The resolution of the machine is about 1 cm^{-1}. Before the experiment the system was calibrated using a silicon standard. Three spectra ranging from 100 to 3700 cm^{-1} were collected for each material, using a 20× objective for 60 s. The spectra were then analysed using a least squares fitting to minimize the residual. The Voigt function was used to model the shape of the peak.

3. Results

The XRD patterns are shown in Fig. 1. Major silicon peaks are indicated by black arrows. These patterns correlate well with ICCD standard hydroxyapatite patterns (PDF number 09-432). No secondary phases were present. Weight fraction and the results of refinements of silicon are listed in Table I. The relative crystallinity were calculated and listed as percentage. For all materials the relative crystallinity was higher than 95%. The HA had highest relative crystallinity and there was no dosage dependence of silicon concentration on relative crystallinity.

A Williamson & Hall plot of (hk0) reflections of different materials is illustrated in Fig. 2. The slope is an estimation of microstrain and the reciprocal of the intercept gives an estimation of the volume average crystal size. Numerical results are listed in Table II. In all cases the microstrain in the hk0 direction was less than 1.0 × 10^{-4}. The dimension along the 00l direction calculated using Scherrer equation is shown in Table III. The size in hk0 direction decreases as silicon concentration increases.

TABLE I Relative crystallinity from Rietveld refinement

	wt% Si	wt% HA	wRp (%)	R_F^2 (%)	Crystallinity(%)
HA 1200	11.2	88.8	10.9	5.9	98.7
0.8 wt%SiHA 1200	13.1	86.9	11.6	4.3	96.6
1.5 wt%SiHA 1200	14.5	85.5	12.4	6.6	95.0
2.0 wt%SiHA 1200	14.1	85.9	10.8	5.4	95.4

TABLE II Crystal size and strain from XRD

	Intercept at $s = 0$	Δ intercept	Crystal size in hk0 (10^3 Å)
HA	1.39*E*–04	2.71*E*–05	5.4 ± 1.0
0.8 SiHA	3.09*E*–04	1.28*E*–04	2.9 ± 0.6
1.5 SiHA	4.78*E*–04	8.17*E*–05	2.0 ± 0.3
2.0 SiHA	7.66*E*–04	1.98*E*–04	1.2 ± 0.3

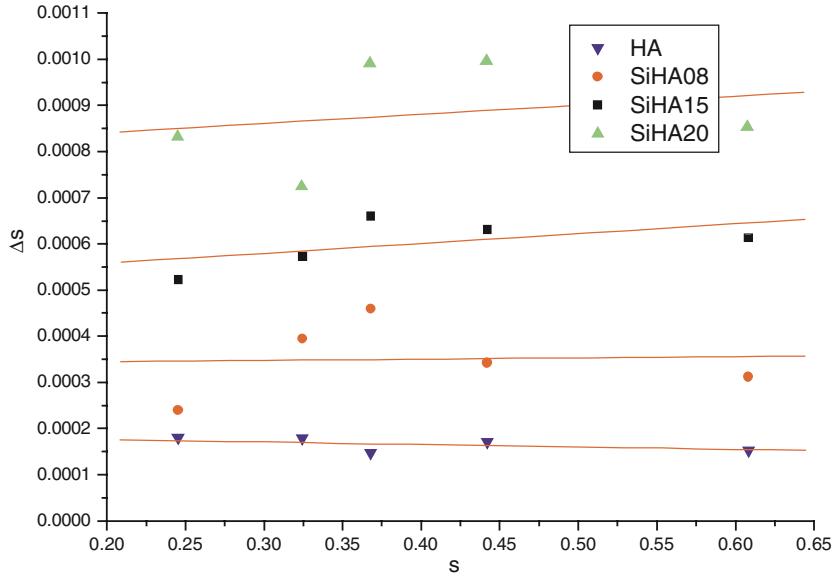

Figure 2 Williamson & Hall plots of (hk0) relections.

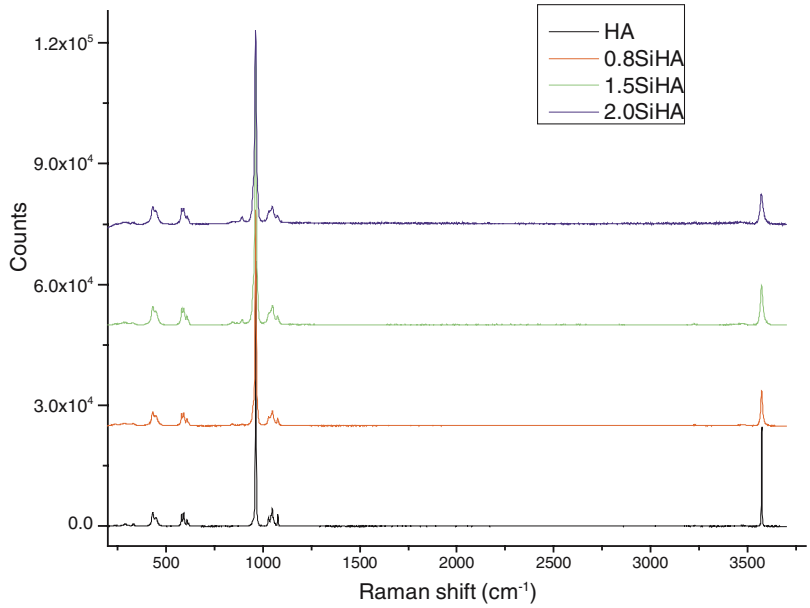

Figure 3 Raman spectrum of HA/SiHA sintered at 1200 °C.

The full Raman spectra of all four different compositions are plotted in Fig. 3. All spectra appear roughly similar except for the slight differences in amplitude of the OH^- stretch mode at 3570 cm^{-1}. PO_4^{3-} bands including the *v*1 mode at 960 cm^{-1}, *v*2 mode between 400–500 cm^{-1}, *v4* mode between 550–650 cm^{-1} and *v3* mode between 1000–1100 cm^{-1} are assigned according to literature [9, 10]. HPO_4^{2-} and CO_3^{2-} vibration modes are absent in all spectra. A detailed observation of these modes is shown in Fig. 4. All peaks were normalized by the amplitude of the PO_4^{3-} *v*1 band. It is obvious that the peaks broadened with silicon substitution. The normalized amplitude of the *v*2, *v*3 and *v*4 increase with silicon substitution in a dose-dependent manner. Three additional bands arise at 845, 890 and 949 cm^{-1}, consistent with previously reported FTIR results [11]. Peaks at 845 and 890 cm^{-1} showed an increase in amplitude with silicon substitution, as shown in Fig. 5. Interestingly, the amplitude of these two modes seems to correlate with each other. As demonstrated in Fig. 5, the summation of the amplitude of both peaks has a much smaller standard deviation than the individual peaks. The new peak centred at 949 cm^{-1} also exhibits a similar dose dependent amplitude (data not shown here).

TABLE III Crystal size along 00l direction (004 diffraction of HA and SiHA has a smaller FWHM than the modelled instrumental function)

	HA (10^3 Å)	SiHA08 (10^3 Å)	SiHA15 (10^3 Å)	SiHA20 (10^3 Å)
002	2.5	2.5	2.3	1.9
004	N/A	N/A	3.6	1.5
006	4.5	3.3	1.5	0.9

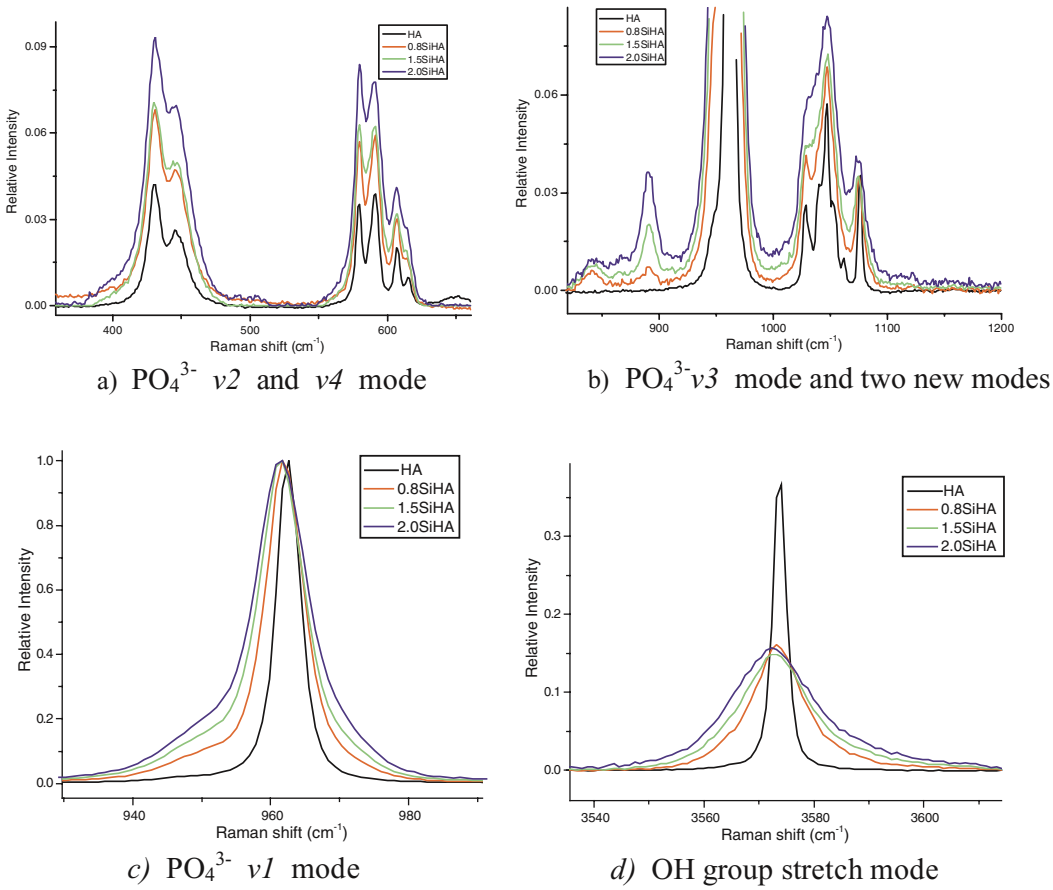

Figure 4 Details of various vibration modes.

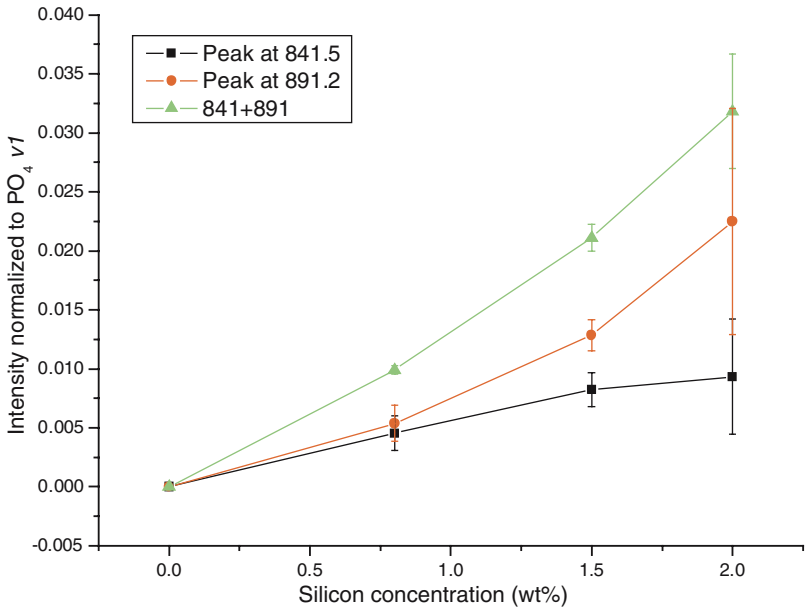

Figure 5 Relative amplitude of peaks at 841.5 and 891 cm^{-1}.

The PO_4^{3-} $v1$ band was evaluated using least squares fitting. This mode was modelled using two peaks in the cases of SiHA as shown in Fig. 6. The statistical results are listed in Table IV. The peak position does not vary significantly with silicon substitution. However, the full width at half maximum and the Lorentzian component of the peak increased steadily with silicon substitution (Table IV) and decrease in crystal size (Fig. 7).

4. Discussion

From the XRD results, a reduction in crystallinity with silicon substitution is evident. However, there appears to be little difference in crystallinity between the different Si-HA samples. The 95–97% crystallinity is consistent with previous reports [12]. The crystal dimension in hk0 direction decreases with silicon substitution. In all cases, the microstrain in the hk0 direction was below the detection limit of our experiment setup (less

TABLE IV Statistical analysis of PO_4^{3-} $v1$ mode (all units are cm^{-1})

	Centre	FWHM	Gaussian component	Lorentzian component
HA	962.6 ± 0.02	4.21 ± 0.06	1.07 ± 0.03	1.31 ± 0.0
0.8SiHA	962.0 ± 0.01	6.48 ± 0.16	1.31 ± 0.02	2.46 ± 0.07
1.5SiHA	961.7 ± 0.1	8.19 ± 0.17	1.41 ± 0.13	3.37 ± 0.06
2.0SiHA	961.3 ± 0.1	9.57 ± 0.26	0.93 ± 0.26	4.50 ± 0.26

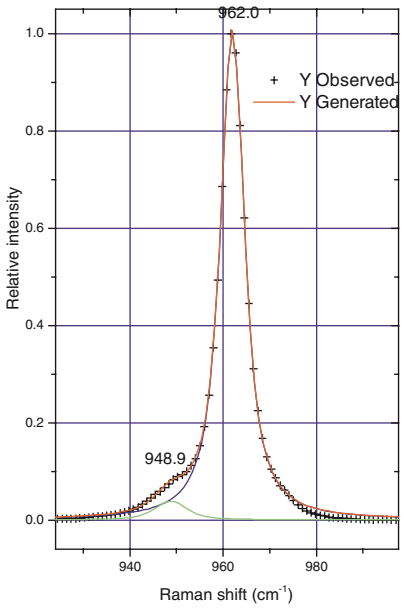

Figure 6 The PO4 $v1$ band of silicon substituted hydroxyapatite.

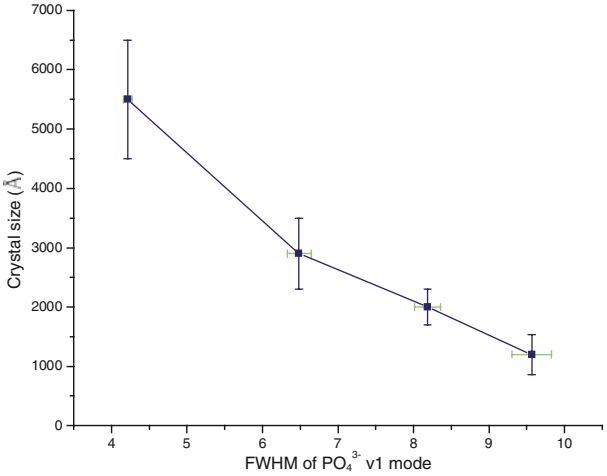

Figure 7 Correlation between crystal size in hk0 and FWHM of PO_4 $v1$ *peak*.

than 1.0×10^{-4}) and therefore it was concluded that the substitution of silicon into the HA lattice did not introduce significant amount of microstrain.

The Raman spectrum of pure HA agreed well with published results [9, 13]. As shown in Figs. 3 and 4, four major PO_4 vibration bands and the OH band at $\sim 3570\,cm^{-1}$ were observed. Furthermore from Fig. 4 we can also exclude the presence of carbonate ions, which are indicated by peaks at 1107 and $1070\,cm^{-1}$ for A type and B type substitution respectively [14]. The PO_4 $v1$ band was a very prominent single peak at $\sim 962\,cm^{-1}$ in all spectra. It is obvious that the peak was broadened in every mode with increasing silicon substitution (Fig. 4). This broadening resulted in overlapping of peaks and also increased the amplitude in the overlapped regions (Fig. 4(a) and (b)). The OH stretch at $3570\,cm^{-1}$ dramatically decreases with the addition of silicon as shown in Fig. 4(d). The drop from HA to Si-HA may be related to the loss of OH groups to maintain electroneutrality and peak broadening. However further silicon substitution did not decrease the amplitude of this peak. The reason for the evolution of OH vibration in the Si-HA series needs to be further studied.

Three additional bands arose at 841, 891 and $949\,cm^{-1}$, consistent with previously reported FTIR results [11]. More interestingly, the intensity of these peaks showed a dosage dependence on silicon concentration. In particular, the summation of two peaks at 841 and $891\,cm^{-1}$ showed an excellent linearity. This dose dependant amplitude may, with careful calibration, provide an alternative method to measure silicon concentration.

A detailed evaluation of the PO_4 $v1$ vibration mode was performed. The PO_4 $v1$ band is a first order internal symmetric stretching mode. In this study the FWHM of this peak increased steadily with decreasing crystal size. Asymmetry was not discovered, possibly concealed by the appearance of the new peak. This phenomenological correlation is shown in Fig. 7. The broadening may therefore be attributed to a number of possible causes. Based on the values obtained in this study, no obvious correlation between the peak broadening and either crystallinity or microstrain was found. The defects and decrease in crystal size can result a broadened peak by breakdown of $q = 0$ selection rule, allowing more phonons to be engaged in the scattering process. The effect of domain size on Raman peaks has been described by well-established phonon confinement model [15, 16]. Theoretical modelling would be very valuable to ascertain the correlation between the broadening and crystal size is reported here. However the quantitative modelling is not currently possible due to the lack of knowledge about phonon dispersion. Therefore other possible source for broadening, e.g. structural disorder, cannot be completely excluded.

Interactions between skeletal tissue and implants are profoundly influenced by dissolution. Ion substitution into the hydroxyapatite lattice can improve biological performance by promoting dissolution [4, 5, 17]. The imperfections from silicon incorporation reported here, may therefore decrease the stability of pure hydroxyapatite and contribute to the enhanced bioactivity of silicon-substituted hydroxyapatite.

5. Conclusion

Crystallinity and crystal size of HA and Si-HA of different substitution levels were measured. All materials were highly crystallized while the crystal size in hk0 direction decreases with silicon substitution. Broadening in Raman peaks and decreases in amplitude of OH group stretch mode vibration were observed. Three new

bands were observed and were assigned to silicon substitution. The correlation between the relative intensity of these peaks and silicon concentration may provide a new method to measure the silicon concentration. The silicon substitution increases the width of the PO_4 $v1$ peak, in particular, the component of Lorentzian character. We propose that broadening is caused by decrease in the crystal size. The imperfections introduced by substitution may contribute to the enhancement in bioactivity of silicon-substituted hydroxyapatite.

Acknowledgments

The authors gratefully acknowledge EPSRC and the Faraday Medical device partnership (GR/S71996/01).

References

1. I. R. GIBSON, J. HUANG, S. M. BEST and W. BONFIELD, *Bioceramics* **12** (1999) 191.
2. N. PATEL, S. M. BEST, W. BONFIELD, I. R. GIBSON, K. A. HING, E. DAMIEN and P. A. REVELL, *J. Mater. Sci. Mater. Med.* **13** (2002) 1199.
3. S. WEINER and W. TRAUB, *Faseb J.* **6** (1992) 879.
4. A. E. PORTER, S. M. BEST and W. BONFIELD, *Bioceramics* **15** (2003) 505.
5. A. E. PORTER, N. PATEL, J. N. SKEPPER, S. M. BEST and W. BONFIELD, *ibid.* **24** (2003) 4609.
6. H. M. RIETVELD, *Acta Crystallographica* **22** (1967) 151.
7. A. C. LARSON and R. B. V. DREELE, "General Structure Analysis System" (Los Alamos National Laboratory, 2000).
8. G. K. WILLIAMSON and W. H. HALL, *Acta Materialia* **1** (1953) 22.
9. S. KOUTSOPOULOS, *J. Biomed. Mater. Res.* **62** (2002) 600.
10. H. OU-YANG, E. P. PASCHALIS, A. L. BOSKEY and R. MENDELSOHN, *Biopolymers* **57** (2000) 129.
11. I. R. GIBSON, S. M. BEST and W. BONFIELD, *J. Biom. Mater. Res.* **44** (1999) 422.
12. I. R. GIBSON, S. M. BEST and W. BONFIELD, *J. Am. Cera. Soc.* **85** (2002) 2771.
13. P. N. DEAZA, F. GUITIAN, C. SANTOS, S. DEAZA, R. CUSCO and L. ARTUS, *Chem. Mat.* **9** (1997) 916.
14. G. PENEL, G. LEROY, C. REY and E. BRES, *Calcif. Tissue Int.* **63** (1998) 475.
15. H. RICHTER, Z. P. WANG and L. LEY, *Solid State Commun* **39** (1981) 625.
16. I. H. CAMPBELL and P. M. FAUCHET, *ibid.* **58** (1996) 739.
17. N. PATEL, I. R. GIBSON, K. A. HING, S. M. BEST, E. DAMIEN, P. A. REVELL and W. BONFIELD, *Bioceramics* **14**(218–212) (2002) 383.

Received 29 June
and accepted 19 August 205